

## OUR RECENT STUDY ON NANOMATERIALS FOR GAS SENSING APPLICATION

Nguyen Van Hieu<sup>(1)</sup>, Hoàng Sĩ Hồng<sup>(2)</sup>, Do Dang Trung<sup>(1)</sup>, Bui Thi Binh<sup>(1)</sup>, Nguyen Duc Chinh<sup>(1)</sup>,  
Nguyen Van Duy<sup>(1)</sup>, Nguyen Duc Hoa<sup>(1)</sup>

(1)International Training Institute for Materials Science, Hanoi University of Science and Technology,

(2)School of Electrical Engineering, Hanoi University of Science and Technology

(Manuscript Received on April 5<sup>th</sup>, 2012, Manuscript Revised May 15<sup>th</sup>, 2013)

**ABSTRACT:** *Recently, novel materials such as semiconductor metal oxide (SMO) nanowires (NWs), carbon nanotubes (CNTs), and hybrid materials SMO/CNTs have been attractively received attention for gas sensing applications. These materials are potential candidates for improving the well known “3S”: Sensitivity, Selectivity and Stability. In this article, we describe our recent studies on synthesis and characterizations of nanomaterials for gas-sensing applications. The focused topics include are: (i) various system of hybrid materials made CNTs and SMO; and (ii) quasi-one-dimension (Q1D) nanostructure of SMO materials. The synthesis, characterizations and gas-sensing properties are dealt thoroughly. Gas-sensing mechanism of those materials, possibility producing new novel materials and other novel applications are also discussed*

**Keywords:** *Carbon nanotubes, Nanowires, Hybrid materials, Gas sensor*

### 1. INTRODUCTION

Nowadays, the gas-sensing field is significant impact in everyday life with different applications such as security of explosive and toxic gases, indoor air quality, industrial process control, combustion control, exhaust gases, and smart house plant in agriculture. Due to the huge application range, the need of cheap, small, low power consuming and reliable solid state gas sensors, has grown over the years and triggered a huge research worldwide to overcome metal oxide sensors drawbacks, summed up in improving the well known “3S”: Sensitivity, Selectivity and Stability [1,2]. A great deal of research effort

has been directed toward the application of nanostructured materials in the gas-sensing field, and a various novel gas sensors have been demonstrated by using different nanomaterials such as carbon nanotubes [3,4], low dimension metal oxides (nanoparticles, nanowires, and nanotubes) [1,2,5] conducting polymer [6]. It has been pronounced that the nanomaterials-based gas sensors can be used to detect various gases with ultra-high sensitivity and selectivity. Accordingly, the toxic gases at concentration of few ppm or even ppb can be easily detected. Especially, few kinds of nanomaterials can be responded to gases at room temperatures.

In this paper, we represent our current studies in the two new class nanomaterials for gas sensing applications. The first one is the hybrid materials, which made of semiconductor metal oxides (SMO) and carbon nanotubes (CNTs), including CNTs-doped SMO and SMO/CNTs composites. It has been realized that special geometries and properties of the hybrid materials offer great potential applications as high performance gas-sensor devices. Previous works have demonstrated that the hybrid materials can be used to detect various gases such as  $\text{NH}_3$ ,  $\text{NO}_2$ ,  $\text{H}_2$ ,  $\text{CO}$ , LPG, and Ethanol [7-12]. These works also reported that the hybrid gas sensors have a better performance compared to SMO- as well as CNTs-based sensors. Interestingly, the composite  $\text{SnO}_2/\text{CNTs}$  and the CNTs-doped  $\text{SnO}_2$  sensors respond to  $\text{NH}_3$  and  $\text{NO}_2$  at room temperature, respectively [9]. This would reduce considerably the power consumption of the sensing-device. The CNTs are hollow nanotube and p-type semiconductor, therefore the improvement of the hybrid CNTs/ $\text{SnO}_2$ -based sensor was attributed to additional nanochannel for gas diffusion and p/n junctions formed by CNTs and  $\text{SnO}_2$  [9]. The second type nanomaterials that we focus on are one-dimension nanostructures of SMO. It has been indicated that the gas sensing application of a new generation of SMO nanostructures such as nanowires, nanorods, nanobles, nanotubes has been extensively investigated [1,13]. These structures with a high aspect ratio (i.e., size confinement in two coordinates) offer better crystallinity, higher integration density, and

lower power consumption [1]. In addition, One-dimensional nanostructures demonstrate a superior sensitivity to surface chemical processes due to the large surface-to-volume ratio and small diameter comparable to the Debye length (a measure of the field penetration into the bulk) [14,15].

## 2. HYBRID MATERIALS FOR GAS SENSING APPLICATIONS

In recent years, we have carried out extensive studies on different kinds of hybrid materials for gas sensors as well as biosensors applications [16-23]. The scope of this paper is only to represent a recent advantage of hybrid materials for gas sensitive materials. We have focused on the development of the hybrid materials made of CNTs and SMO nanoparticles for gas-sensing applications.

### 2.1. $\text{TiO}_2$ and $\text{SnO}_2$ doped with carbon nanotubes

Pt-Nb co-doped materials have been previously investigated. It was found that the  $\text{TiO}_2$  gas-sensing material has some advantages over  $\text{SnO}_2$  materials. However, the former has very low response at low operating temperatures (lower than  $300^\circ\text{C}$ ). This is difficult to overcome by using noble metals dopants such as Nb, Pt and Pd. In this section, we show a response improvement of  $\text{TiO}_2$ -based sensor by using CNTs as dopant. First, we have tried to add the SWCNTs into the Nb-Pt doped  $\text{TiO}_2$  material for gas-sensing characterizations.

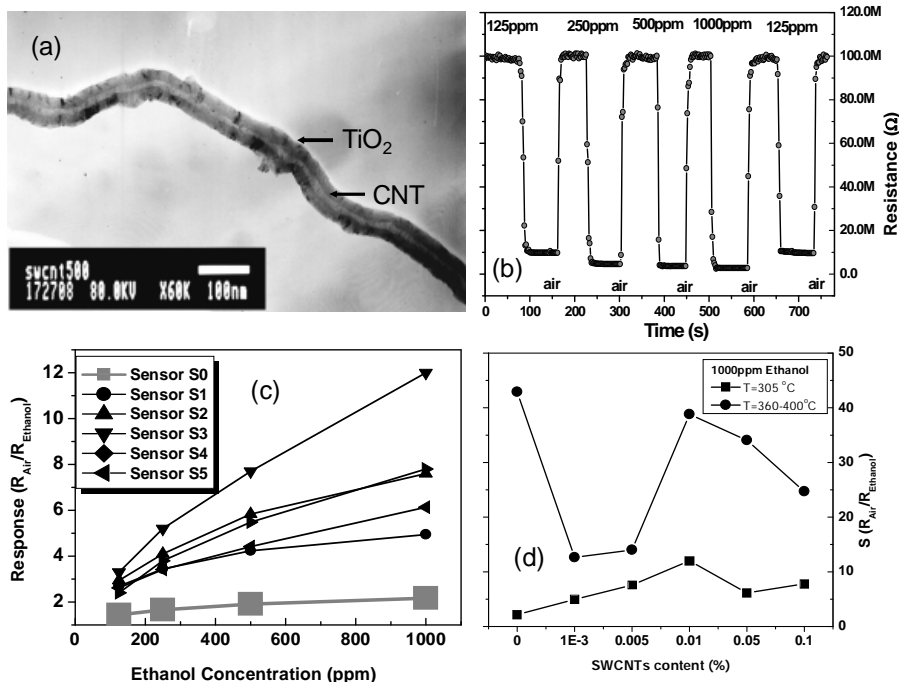


**Figure 1.** TEM image of morphology of CNTs-doped TiO<sub>2</sub> (a), Transient response of CNTs-doped TiO<sub>2</sub> sensor to a serial ethanol concentrations (b), sensor response versus ethanol concentration (c), sensor response versus SWCNTs-doped TiO<sub>2</sub> (d) [16].

The sol of (1%wt)Nb-(0.5% wt) Pt co-doped TiO<sub>2</sub> was prepared by so-gel method. The precursors used to made the solutions were Ti(OC<sub>3</sub>H<sub>7</sub>)<sub>4</sub> (99%), PtCl<sub>6</sub>.xH<sub>2</sub>O (99.9%), Nb(OC<sub>2</sub>H<sub>5</sub>)<sub>5</sub> (99%) and C<sub>3</sub>H<sub>7</sub>OH (99.5%). As obtained CNTs-doped TiO<sub>2</sub> material is shown in Fig. 1a. It can be seen that bundle SWCNTs with diameter around 10 nm surrounded by TiO<sub>2</sub> nanoparticles. Fig. 1b. shows the response and recovery times of the sensor are less than 5s at the operating temperature of 380°C. The sensor response is repeated with the same ethanol concentration after several cycles of the gas-injection. The sensitivity of CNTs-doped TiO<sub>2</sub> sensors versus operating temperatures is shown in Fig. 1c. The S0, S1, S2, S3, and S4

sensors were corresponded to 0.0, 0.001, 0.005, 0.01, 0.1 wt% of SWCNTs doping on Nb-Pt co-doped TiO<sub>2</sub> sensor. It can be seen that the operating temperature is an obvious influence on the sensitivity of all sensors to ethanol gas and the sensitivity of Nb-Pt co-doped sensor increases more steeply compared to that of the hybrid SWCNTs/Nb-Pt co-doped sensors. From Fig. 1d, it is can be seen that the response to ethanol of SWCNTs/Nb-Pt co-doped sensor is increased at first as SWCNTs content increases up to 0.01% but it is reduced when SWCNTs is further increased to 0.1%. This does not observe for the operating temperature of 380°C. More detail on this work can be found elsewhere [16].

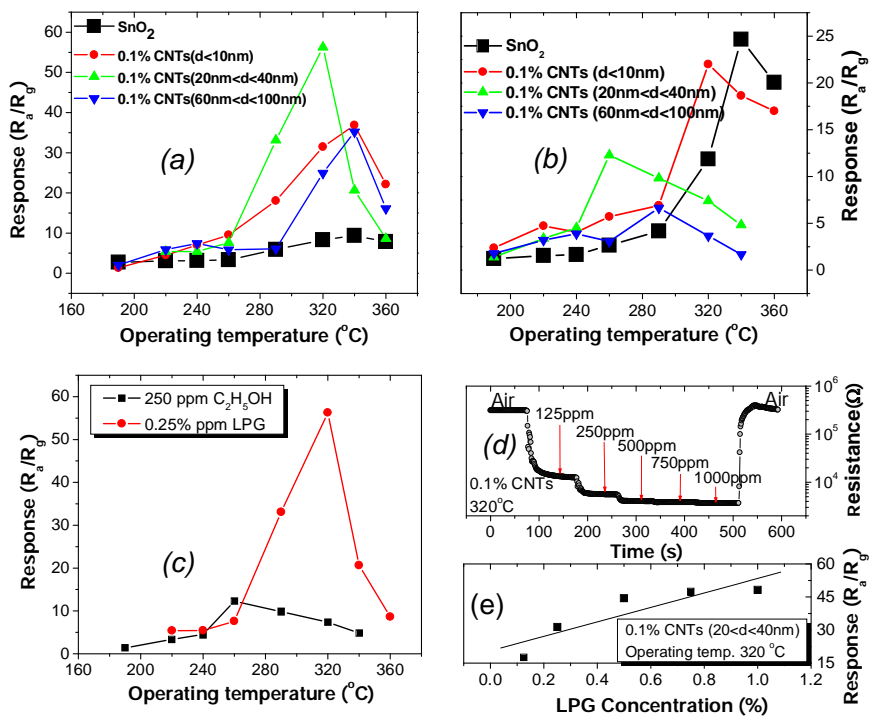


**Figure 2.** Response of MWCNTs (with  $d<10\text{nm}$ ;  $20\text{nm}<d<40\text{nm}$ ;  $60\text{nm}<d<100\text{nm}$ ) -doped  $\text{SnO}_2$  sensors to LPG (a) and ethanol gas (b); the response to ethanol gas and LPG (c); step wise decrease in resistance obtained with increasing ethanol concentration from air to 1000 ppm ethanol gas in air for (0.1wt%) MWCNTs-doped  $\text{SnO}_2$  sensors operating at  $240^\circ\text{C}$ ; (e) the response versus LPG concentration with linear fit [17].

In this section, the sensing properties of blank and CNTs doped  $\text{SnO}_2$  sensor have been investigated for comparison. All results of this work were summarized in Fig.2. It can be recognized that the responses to ethanol gas and LPG of all MWCNTs-doped  $\text{SnO}_2$  sensors are improved at low region of operating temperatures. Especially, we can see that MWCNTs-doped  $\text{SnO}_2$  sensor shows to be more selective to LPG than to ethanol gas at operating temperature range of  $280\text{--}350^\circ\text{C}$ . This effect is completely different with the metal oxides-doped  $\text{SnO}_2$  sensors. Fig. 2d depicts the electrical resistance variations

obtained with several steps of different LPG concentration from air to 1% LPG in air for the (0.1 wt%,  $d<10\text{nm}$ ) MWCNTs-doped  $\text{SnO}_2$  sensor operating at  $320^\circ\text{C}$ . Similar to the PtO<sub>2</sub>-doped  $\text{SnO}_2$  sensor in the detection of ethanol, the MWCNTs-doped  $\text{SnO}_2$  sensor shows a good reversibility in the detection of LPG and the stepwise decrease of electrical resistivity of the MWCNTs-doped  $\text{SnO}_2$  film is very consistent with the increasing amount of LPG oxidation. More LPG oxidation caused the introduction of more electrons into the  $\text{SnO}_2$  surface and the film became less resistive.

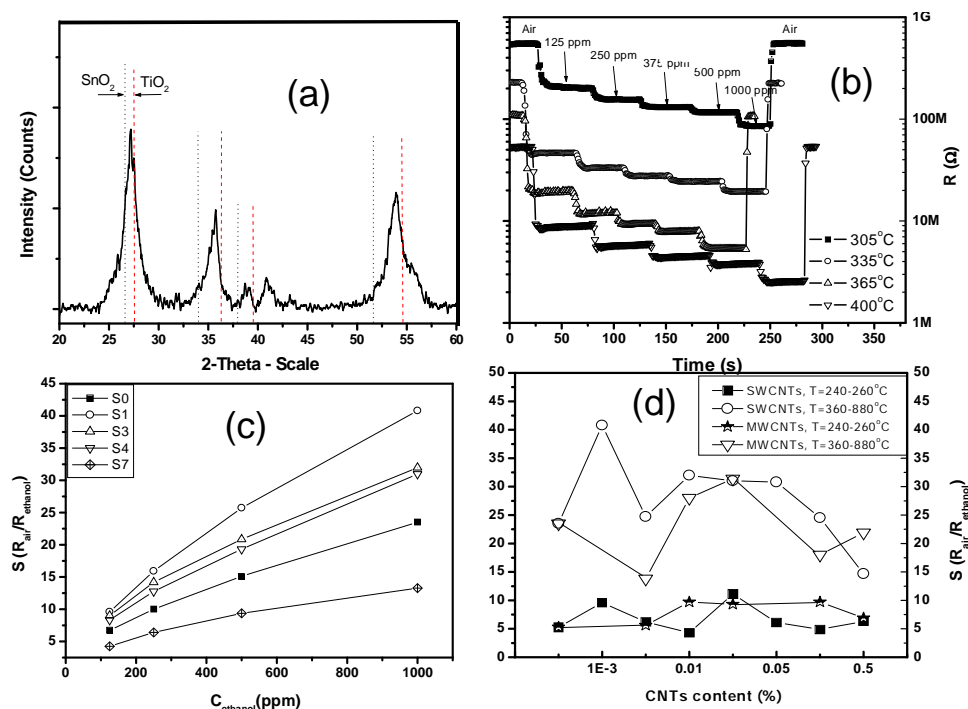


**Figure 3.** X-ray diffraction pattern of SnO<sub>2</sub>-TiO<sub>2</sub> shows the peaks of solid solution (a); sensor response to a serial of ethanol concentration at different temperatures (b); response versus on ethanol concentration characteristics in the range from 125 to 1000ppm at operating temperatures of 240°C; sensor response versus MWCNTs and SWCNTs inclusion content [18].

Fig. 2e depicts the variation of sensitivity with LPG concentration in air for the MWCNTs-doped SnO<sub>2</sub> sensor at operating temperature of 320°C. The sensitivity seems to be linear in the concentration range 0.1 – 0.6% of LPG in air and saturates thereafter. The 90% response time for gas exposure ( $t_{90\%(\text{air-to-gas})}$ ) and that for recovery ( $t_{90\%(\text{gas-to-air})}$ ) were calculated from the resistance-time data shown in Fig. 2d. The  $t_{90\%(\text{air-to-gas})}$  value is around 21 s, while the  $t_{90\%(\text{gas-to-air})}$  value is around 36 s. It can be seen that the response times of the Pt- and MWCNTs-doped SnO<sub>2</sub> sensors are similar, while the recovery time of MWCNTs-doped sensor is relatively shorter than that of the Pt-

doped SnO<sub>2</sub> sensor. More detail on the gas-sensing mechanism and explanation can be found from our recent publication [18].

It has been reported that the mixed oxide has been extensively studied to combine the advantages of sensing property of each oxide component. We have also explored possibilities to improve the performance and to reduce the operating temperature of the SnO<sub>2</sub>-TiO<sub>2</sub> ethanol sensors by adding CNTs. SnO<sub>2</sub>-TiO<sub>2</sub> sol was also prepared by so-gel method. The precursors used to fabricate the solutions were Tetra Propylortho Titanate Ti(OC<sub>3</sub>H<sub>7</sub>)<sub>4</sub> (99%), Tin ethylhexanoate Sn(OOCC<sub>7</sub>H<sub>15</sub>)<sub>2</sub>, and Isopropanol C<sub>3</sub>H<sub>7</sub>OH (99.5%). The formation

of SnO<sub>2</sub>-TiO<sub>2</sub> solid solution was obtained that can be observed from XRD pattern in Fig.3a. With the mole ratio of SnO<sub>2</sub>:TiO<sub>2</sub> at 3:7, it shows that the diffraction peaks of oxide solution follow Vegard's law. In this study, we have measured responses of all sensors to ethanol gas at different concentrations in a range from 125 to 1000 ppm and at operating temperatures in a range from 210 to 400°C to investigate the gas-sensing properties. The sensor responses at various operating temperatures are shown in Fig. 3b. It was found that the response and recovery times of the sensors are less than 10 s. We have observed that the metal oxide thin film sensor have already shown a relatively low response-recovery time, and the hybrid CNTs/metal oxide thin film sensor have shown even lower values than that. The dependence of the response on ethanol concentration at operating temperatures of 260 and 380°C is given in Fig. 3c. It can be seen that all the sensors present more or less linear characteristic in the investigated range from 125 to 1000ppm ethanol, which makes their use more convenient. Once again, S1 and S4 dedicate the best in slope than the others. It can be seen from Fig. 3d that optimized CNTs content seems to be around 0.01% wt to obtain the best performance sensor. More interested results can be found from our recent publication [17].

## **2.2. SnO<sub>2</sub>/CNTs and polypyrrole/CNTs composites for room temperature gas sensors**

Room temperature gas sensors based on organic or inorganic materials/CNTs composites seem significantly meaning exploration. The composite of SnO<sub>2</sub>/CNTs were prepared by very simple route, the commercial SnO<sub>2</sub> nanoparticles and CNTs were mixed each other, using CTAB surfactant and immersion-probe ultrasonic. Morphology of the SnO<sub>2</sub>/CNTs composite was characterized by FE-SEM, it was found out that the CNTs disperse well and separate from each other clearly (see, Fig.4a) and CNTs are well embedded by spherical tin oxide nanoparticles. Our sensing element is of a thin film type. Therefore, the morphology of the composite thin film after the heat treatment at 550°C in the vacuum was also verified by FE-SEM, and the result is shown in Fig. 4b. It is observed that there are many fibers-like protrusions emerged from the SnO<sub>2</sub> matrix, which may indicate that the CNTs are most embedded in the SnO<sub>2</sub>. The CNTs on the surface are also coated by SnO<sub>2</sub> nanoparticles as indicated in the inset of Fig. 4b. Fig. 4c is to show estimations of the response and recovery times of our best sensor, in which optimized parameters such as MWCNTs content, thermal treatment condition and thickness were selected. In this figure, the time interval between measured points is 2 s. It can be seen that the response-recovery time is less than 5 min. Fig. 4c also shows that the response occurred immediately after few seconds of gas injection in the chamber.

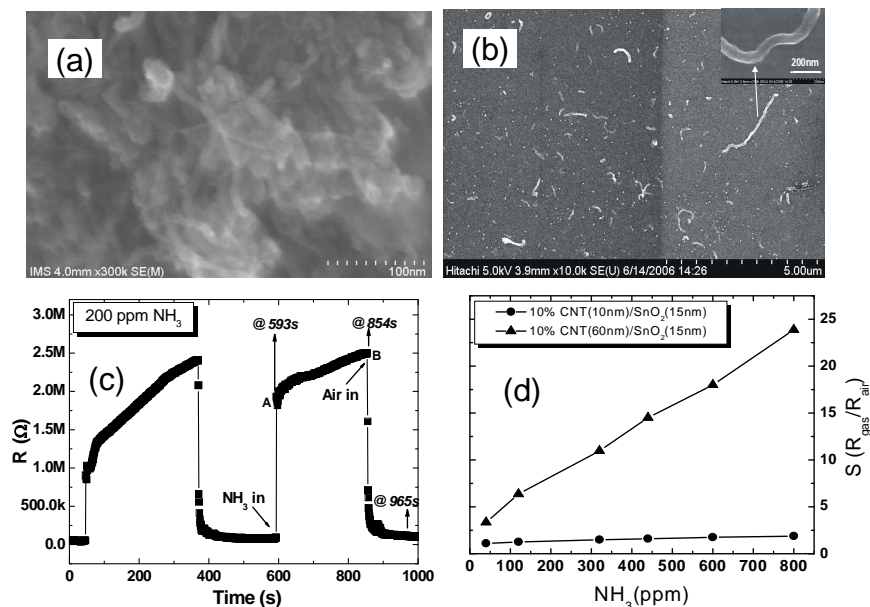


**Figure 4.** SEM images of SnO<sub>2</sub>-(10%wt)MWCNTs powder (a) and thin film (b) nanocomposites annealed at 550°C in the vacuum at 10<sup>-2</sup> torr; a dynamic response of the composite sensor to NH<sub>3</sub> gas at room temperature (c); the sensor response versus NH<sub>3</sub> concentration for the composite using CNTs with diameter (d) [19].

The response time from A to B (Fig. 4c) is the time needed for the gas in the testing chamber to become homogenous. It was shown that the diameter of CNTs strongly affected the electronic properties as well as gas-adsorption/desorption behavior. Therefore, in this work, we also studied the effect of MWCNTs diameter on the response of the MWCNTs/SnO<sub>2</sub> composites-based sensor. Fig. 4d shows the response of two composite sensors, which were fabricated by using MWCNTs with diameters of lower than 10 nm and in the range of 60–100 nm. We observe that the composites using MWCNTs with the larger diameter has higher response. Other effect such as film thickness, CNTs content, and heat-treated temperature were already

investigated that can be found further in [19]. Conducting polymer and CNTs composite has been also extensively investigated, because the conducting polymer itself can be used to detect the various gases at room temperature. The PPY/SWCNTs and PPY/MWCNTs composites-based sensors have been already developed for detection of ethanol and NH<sub>3</sub>, respectively, and they have shown a higher sensitivity than both PPY- and CNTs-based sensors separately over a wide range of gas concentrations at room temperature. We have developed PPY/SWCNTs nanocomposite-based sensor for detection of NH<sub>3</sub> gas at room temperature with good sensitivity and relatively fast response-recovery.

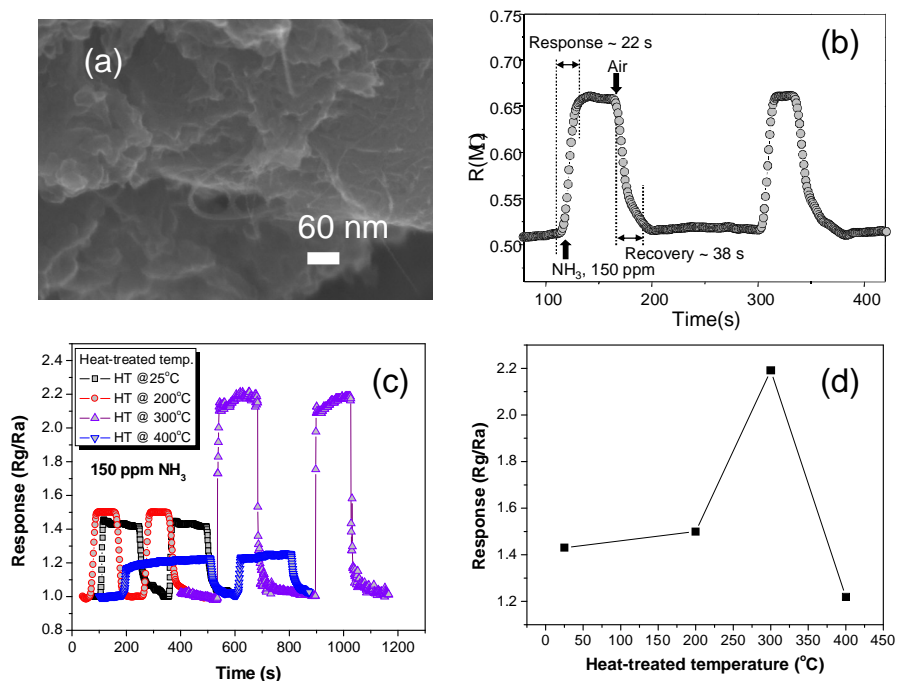


**Figure 5.** FE-SEM image of PPY/SWCNTs nanocomposite (a); Response curve of SWCNTs/PPY composite sensor to  $\text{NH}_3$  at room temperature (b); the  $\text{NH}_3$  gas sensing characteristic of PPY/SWCNTs composite at different operating temperature, transient responses of the sensor to 150 ppm  $\text{NH}_3$  (c); the sensor response as a function of operating temperature (d) [20].

The gas-sensitive composite thin film was prepared by using chemical polymerization and spin-coating techniques. The morphology of as-synthesized PPY/SWCNTs composite (see Fig. 5a) shows that the SWCNTs are well-embedded within the matrix of the PPY. The FT-IR spectra (not show) and FE-SEM characterizations are to confirm that the as-synthesized SWCNTs/PPY nanocomposite prepared in the present work are similar with the carbon nanotubes/PPY composites prepared by previous reports such as chemical polymerization, vapor phase polymerization [20], and electrochemical polymerization. Fig. 5b shows a typical response curve of the thin film SWCNTs/PPY composite gas sensors

during gas-sensing at room temperature. The response curve indicates that the resistance signal varies with time over the two of cyclic tests. Before each cyclic test, the sensor was exposed to air and the measured resistance of the sensor was equal to  $R_a$ . At the beginning of each cyclic test, a desired  $\text{NH}_3$  gas was injected the chamber (4L). The measured resistance changed gradually. After a certain time, the resistance was changed very slowly, almost reaching a stable value,  $R_g$ , corresponding to the response of the sensor to  $\text{NH}_3$  gas. Then, the glass chamber was removed from the sensor to expose the sensor to air again. The measured resistance was restored to its original value,  $R_a$ . The 90% response time for gas

exposure ( $t_{90\%(air-to-gas)}$ ) and that for recovery ( $t_{90\%(gas-to-air)}$ ) were calculated from the resistance–time data shown in Fig. 3. The  $t_{90\%(air-to-gas)}$  values is around 22s, while the  $t_{90\%(gas-to-air)}$  value is around 38s. It was found that these values are lower than those of both the PPY- and the CNTs-based  $NH_3$  gas sensors reported in the literature. Although the aim of this work is to developed room temperature gas sensors for  $NH_3$  detection, we have tested the composite sensor to 150 ppm  $NH_3$  at different temperatures such as 25, 40, 50°C for examining the effect of operating temperature on the sensitivity to  $NH_3$  gas and finding optimized operating temperature. The obtained responses of the composite sensor are shown in Figure 5e. It turns out that the sensor response is significantly decreased with increasing the operating temperatures (see Figure 5e). We have also tested the composite sensor at temperature of 100 °C, we have found that the sensor is not response with  $NH_3$  gas (not show). The effect of film thickness, heat-treated temperatures, CNTs content and  $NH_3$  gas concentration was already investigated that can be found elsewhere [20].

### 2.3. $La_2O_3$ /CNTs co-doped $SnO_2$ sensor for highly sensitive ethanol gas sensor

CNTs/ $SnO_2$  hybrid materials doped with catalytic materials such Pd, Pt,  $RuO_2$ ,  $La_2O_3$  could be new exploration for improving the selectivity and sensitivity of the hybrid materials. We have been realized that the

$La_2O_3$ -doped  $SnO_2$  sensor has very high sensitivity to ethanol gas [21]. We studied the influence of CNTs addition on the sensing properties of  $La_2O_3$  doped  $SnO_2$  materials. Hydrothermal method was used to prepare  $SnO_2$  nanoparticles and  $SnO_2$  nanoparticles with CNTs inclusion sols. The thick sensing films were deposited on the alumina substrate by drop-coating and their gas sensing behaviors to ethanol and other reducing gases such as acetone, propane, CO, and  $H_2$  have been investigated. The  $La_2O_3$ - and CNTs/ $La_2O_3$ -doped  $SnO_2$  sensors exhibited a selective detection to ethanol gas as shown in Fig 6a and 6b. It can be seen that the  $La_2O_3$ -deoped  $SnO_2$  sensor has good sensitivity and selectivity to ethanol gas over various gases such as  $C_3H_8$ , CO and  $H_2$ , and CNTs/ $La_2O_3$  co-doped sensor has shown even better (seen Fig 6b). We have carefully tested the ethanol gas, and it was shown that the sensitivity of CNTs/ $La_2O_3$  co-doped sensor is steeply increased with ethanol gas concentration. It is much more meaning when tested with higher ethanol concentrations (higher than 200 ppm) as shown in Fig. 6c.

### 2.4. Gas sensing mechanism of CNTs/ $SnO_2$ hybrid materials

The improvement of the SMO gas-sensor performance by including of SWCNTs and SMO/CNTs composite have not been well understand so far and not much literature has reported on the relative work.

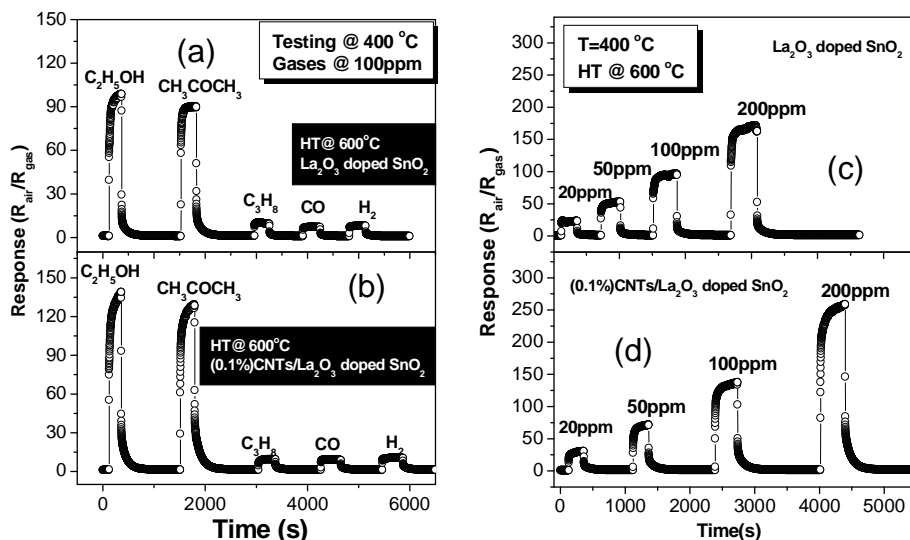


**Figure 6.** Sensor response of SnO<sub>2</sub> doped with La<sub>2</sub>O<sub>3</sub> and co-doped with CNTs to different gases (a, b) and to various ethanol concentration gas (c,d) [21].

The model proposed by B.-Y. Wei and et al. [9] seems to be reasonable for the explanation. This model was applied for SWCNTs doped SnO<sub>2</sub> somehow, we can apply for our case. The model has been hypothesized that CNTs/SnO<sub>2</sub> sensor can build up p/n heterojunctions, which was formed by (n-oxide)/(p-CNT)/(n-oxide). Fig.7a schematically depicts the changes of the electronic energy bands for two depletion layers, one is on the surface of mixed oxide particles, and the other is in the interface between CNT and mixed oxide. When the mixed oxide is exposed to ethanol gas, ethanol molecules will react with oxygen ions on the surface of mixed oxide. This can simply be described as



The electrons released from the surface reaction transfer back into the conduction bands, which increase the conductivity of the sensing material. It is noted that the adsorption

of the ethanol gas may change the two depletion layers as described above. Before the ethanol gas is adsorbed, the widths of the depletion layers at the interface between SMO grains and SMO/CNT are given by  $d_2$  and  $d_4$ , respectively. After adsorption, the widths of these depletion layers are  $d_1$  and  $d_3$ , respectively. Both these effects change the depletion layers at the n/p junction of the sensing material, which can explain the much improved sensitivity. Simply speaking, n-type SMO and p-type CNT form a hetero-structure. Like the working principle of an n-p-n amplifier, carbon nanotubes work as a base, blocked electrons transfer from n (emitter) to n (collector) and thus lower the barrier a little bit, allowing a large amount of electrons to pass from emitter to collector. This amplification effect can be explained by the hybrid materials (SnO<sub>2</sub>/SWCNTs) can detect NO<sub>2</sub> at room temperature [9]. So the improvement of the gas

sensor performance and the shift of operation temperature toward lower temperature region from our work can attribute to the amplification effects of junction combined with gas reaction. This can be also a reason to explain the SnO<sub>2</sub>/CNTs sensor can detect NH<sub>3</sub> at room temperature. Further more, it should be noted that the CNT is perfect hollow nanotube with a diameter in order of nanometer. These nanotubes embedded in SMO film will provide an easy diffusion for chemical gas accessing

through over the bulk material. After the thermal treatment, these tiny CNTs were left in the bulk material derived to form the permanent gas nanochannels as shown in Fig. 7b. The use of CNTs can bring some advantages such as introducing identical open gas nano-channel through bulk material, achievement of a great surface to volume ratio, and providing good gas-adsorption sites due to inside and outside of CNTs.

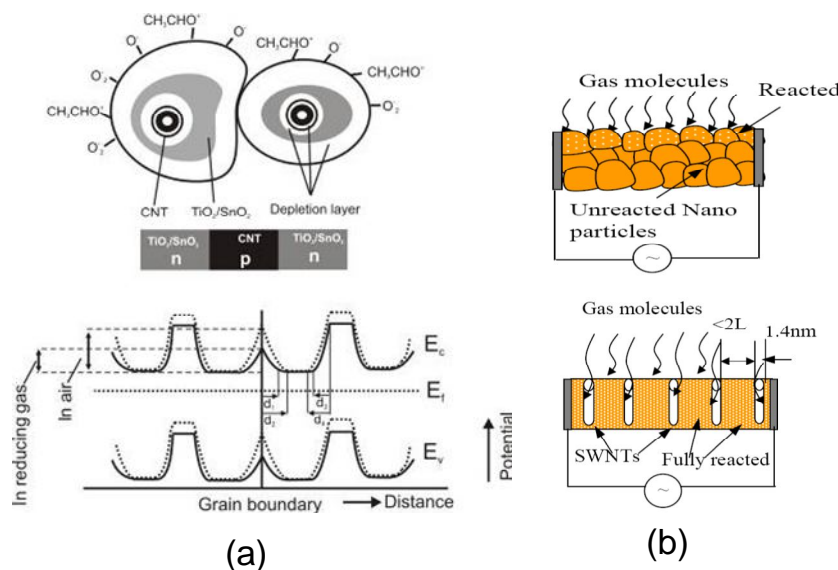


**Figure 7.** Schematic of potential barriers to electronic conduction at grain boundaries and at p-n heterojunctions for CNTs/SMO; d1 and d3 are depletion layer widths when exposed to ethanol; d2 and d4 are depletion layer widths in air (b); nanochannel forming the SMO materials (b) [18].

### 3. NANOWIRES MATERIALS FOR GAS SENSING APPLICATIONS

Various kinds of one-dimensional metal oxides such as ZnO, SnO<sub>2</sub>, WO<sub>3</sub>, CuO, and TiO<sub>2</sub> have been investigated for gas sensing applications. Appropriated nanowires are

investigated for particular gas sensors [24-31]. However, in this paper we focused on the ZnO and SnO<sub>2</sub> nanowires-based sensor. The important technologies related to these gas sensors are presented.

### 3.1. Low dimension ZnO nanostructures for ethanol sensor

Recently, quasi-one-dimensional (Q1D) ZnO nanostructures, such as nanowires, nanobelts and nanoneedles, have been attracting tremendous research interests and they have been emerging as candidates for above-mentioned applications with much better performance and building up new generation of nanoscale devices. The Q1D ZnO nanostructures can be synthesized by various methods such as arc discharge, laser ablation, pyrolysis, electrodeposition, and chemical or physical vapor deposition. However, the most

common method to synthesize ZnO nanostructures utilizes a vapor transport process based on the so-called vapor-liquid-solid (VLS) mechanism of anisotropic crystal growth. Our work has focused on the synthesis of ZnO nanostructures at relative low temperature that can be combined with microelectronic fabrication process. Recently, we have successfully prepared ZnO nanostructures at temperature range 550-600°C. The gas sensor devices were fabricated by directly growing the ZnO nanostructures on interdigitated electrodes with previously depositing Au catalytic layer (see Fig. 8a).

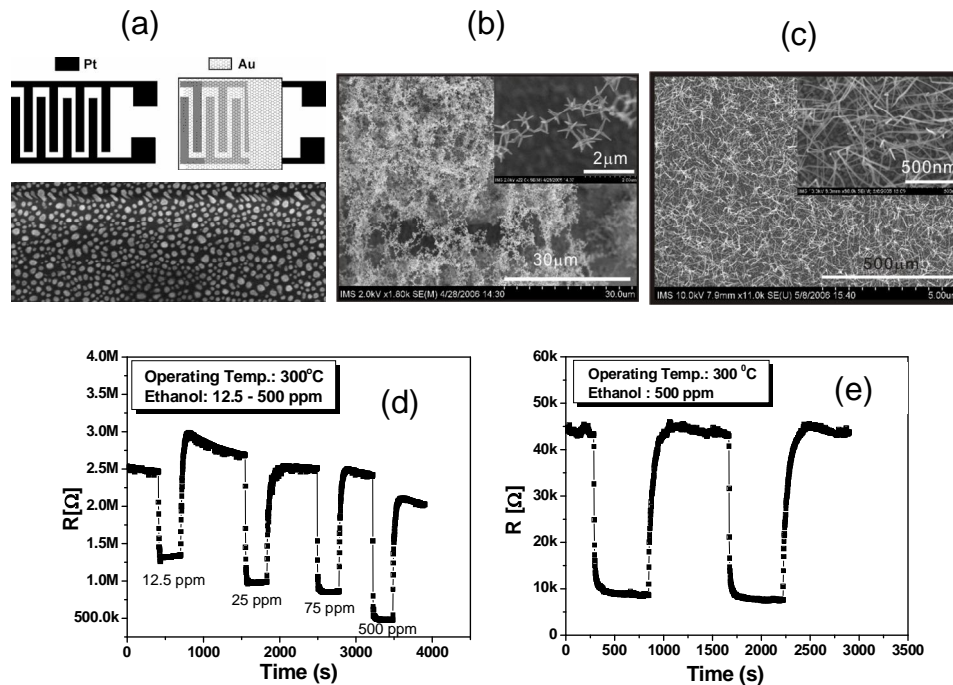


**Figure 8.** Interdigitated electrode with Au catalysis layer on the top (a); The ZnO nanotetrapods (b) and nanowires grown on the electrode; ethanol response of ZnO nanotetrapods- and nanowires -based sensors (d, e)[24].

ZnO nanotetrapods- and nanowires-based sensors were fabricated by thermal evaporation

method at temperatures of 600°C and 550°C as shown in Fig. 8b and 8c. The detail of the

synthesis process can be found elsewhere [24]. The ethanol response of these sensors was measured at temperature of 300°C that indicated in Fig. 8d and 8e. The sensor response to 500 ppm ethanol of nanotetrapods-based sensor was found out to be about 5.3. The response and recovery times were determined as the time to reach 90% of the steady state signal when the sensor was taken from air to a

sample gas and from a sample gas to air, respectively. The response and the recovery times were found to be less than 25 s. The sensor response of as-obtained ZnO nanowires-based sensor is relatively lower than the nanotetrapods-based sensor. This can be attributed to the low-density of nanowires grown on the electrodes.

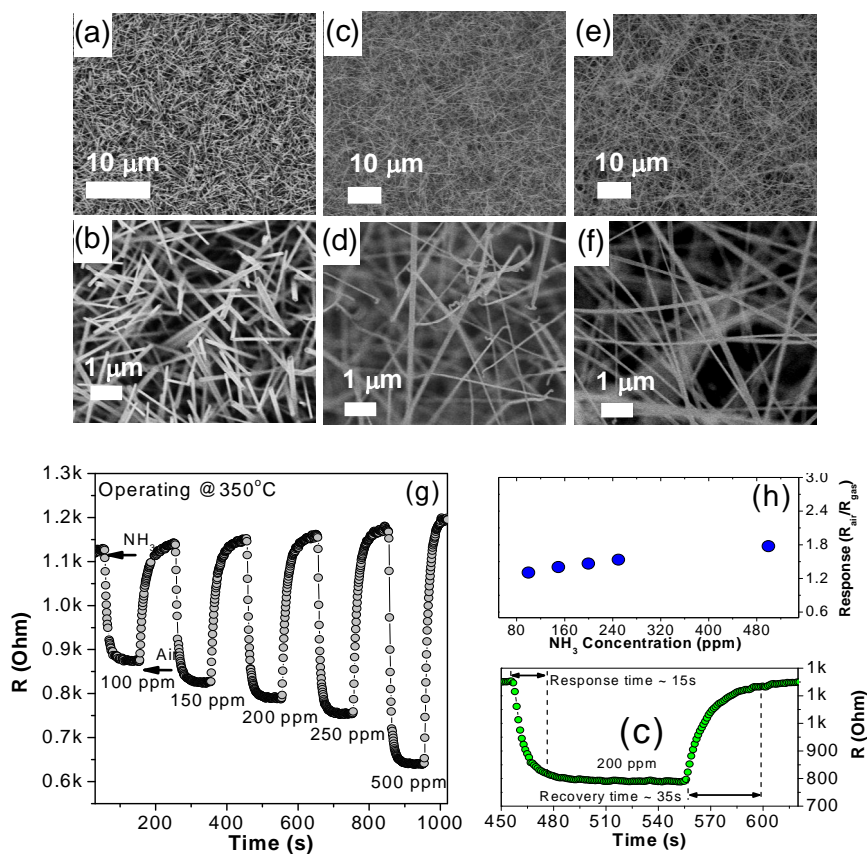


**Figure 9.** ZnO NWs synthesised at temperatures of 850°C (a, b), 900°C (c, d) and 950°C (e, f); Response transients of the ZnO NWs sensors synthesised at 950°C to 100–5000 ppm NH<sub>3</sub> (g); the sensor response as a function of NH<sub>3</sub> gas concentration (h); the estimation of response and recovery times (i)[25].

Recently, we have successfully synthesized ZnO at higher temperatures using thermal

carbon reduction method. The ZnO NWs were synthesized by using our home-made thermal

CVD set-up. The detail synthesis process can be found elsewhere [25]. Figure 9(a, b), (c, d) and (e, f) shows the FE-SEM image of the ZnO NWs synthesized at temperatures of 850, 900, and 950°C, respectively. The samples grown at different temperatures have different morphologies. As shown in Figure 9a, high-density ZnO NWs are obtained at a low temperature of 850°C, and the length of the NWs ranges from 2 to 4 μm with diameters ranging from 50–150 nm (Fig. 9b). As seen from Fig. 9c and 9e, the ZnO NWs synthesized at higher temperatures are of longer length, which is at about 10–20 μm. Their diameters do not differ much from the previous sample. As for the carbothermal reduction process, ZnO NWs can be synthesized under an inert atmosphere using Ar gas.

However, we found that it is very difficult to synthesize ZnO NWs under the flow of Ar gas alone. Our experiment indicates that the ZnO NWs are only successfully synthesized by adding the O<sub>2</sub> gas at a flow of 0.5 sccm with Ar gas flowing at a rate of 50 sccm. Moreover, it was revealed that the synthesis of ZnO at a low-temperature process (<550°C) has low reproducibility compared with the one at high-temperature process (<950°C) (not shown here). In order to characterize gas-sensing properties of ZnO NWs, the sample synthesized at 950°C was chosen for gas sensor fabrication. As-fabricated ZnO NWs sensors were tested with various NH<sub>3</sub> gas concentrations from 100 to 500 ppm at a working temperature of 350°C. The transient

response of the sensor to NH<sub>3</sub> gas is shown in Fig. 9g. It can be seen that the response to NH<sub>3</sub> gas varies from 1.3 to 1.8 for the NH<sub>3</sub> gas concentration range (see Fig. 9h). Oxygen sorption plays an important role in electrical transport properties of ZnO NWs. Furthermore, oxygen ionosorption removes conduction electrons and thus lowers the conductance of ZnO. Hence, the sensing mechanism of ZnO to NH<sub>3</sub> gas may be described as follows. When ZnO NWs sensor is exposed to a reductive gas at a moderate temperature, the gas reacts with the surface oxygen species of the NWs, which decreases the surface concentration of O<sub>2</sub><sup>-2</sup> ions and increases the electron concentration. This eventually increases the conductivity of the ZnO NWs. However, in the case of ZnO thin films, the charge state modification takes place only at the grain boundary or porous surface. In the case of ZnO NWs, it is expected that the electronic transport properties of the entire ZnO NWs will change effectively due to the gas adsorption. In this light, the NWs can be considered as promising materials for sensors to detect other gases. Various catalytic materials coated on the ZnO nanostructures can improve the selectivity of the gas sensors. This aspect is currently being studied by our group as well as by many others. As shown in Figure 9i, the measured resistance was restored to its original value, R<sub>a</sub>. The 90% response time for gas exposure ( $t_{90\%(\text{air-to-gas})}$ ) and that for recovery ( $t_{90\%(\text{gas-to-air})}$ ) were calculated from the resistance–time data (Figure 9i). The  $t_{90\%(\text{air-to-gas})}$  value is around 15 s, while the  $t_{90\%(\text{gas-to-}}$

air) value is around 35 s. These response and recovery times are relatively shorter than that

reported previously in [33].

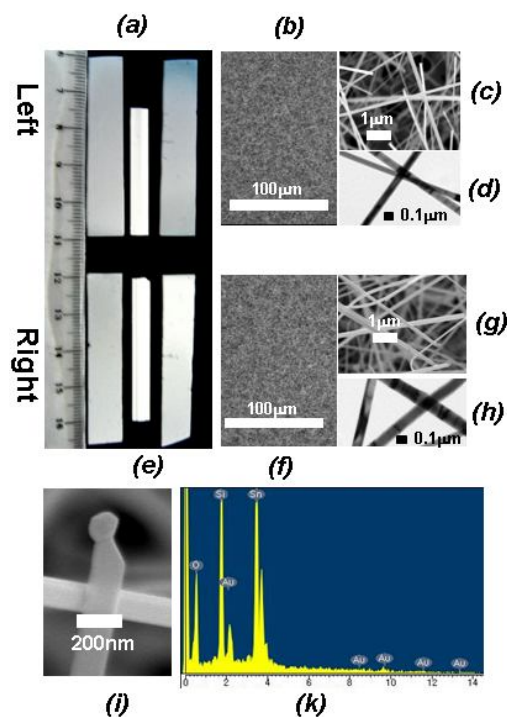


**Figure 10.** Optical microscopes image of SnO<sub>2</sub> NWs on the Si and Al<sub>2</sub>O<sub>3</sub> substrates (a, e), FE-SEM and TEM images of SnO<sub>2</sub> NWs (b, c, d, g, h, f) obtained on the left and right of source, (i) SnO<sub>2</sub> nanowires with Au catalyst cap, and (k) EDX spectrum measured at the catalyst cap [27].

### 3.2. Synthesis a large scale SnO<sub>2</sub> nanowires for gas sensor applications

Although many different Q1D nanostructures of SMO such as SnO<sub>2</sub>, ZnO, In<sub>2</sub>O<sub>3</sub>, WO<sub>3</sub> and TiO<sub>2</sub> have been investigated for their gas sensing properties, researchers have paid greater attention to SnO<sub>2</sub> nanowires (NWs)-based sensors because their counterparts such as a thick film, porous pellets and thin films are versatile in being able to sense a variety of gases and are commercially

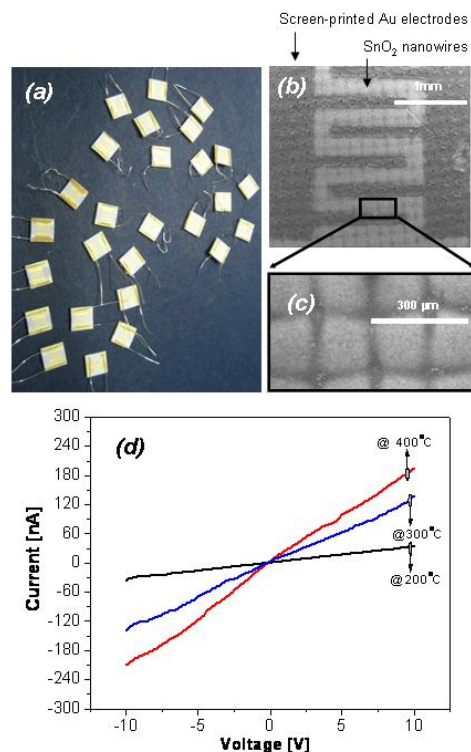


**Figure 11.** As-fabricated gas sensors (a,b,c) and I-V characteristic of the sensors at different temperatures (d) [27].

available. In the light of that we have carried out an intensive study on the synthesis SnO<sub>2</sub> nanowires materials for gas sensing applications. So far we are very successful in the synthesis SnO<sub>2</sub>NWs materials. We have developed a good recipe for synthesizing SnO<sub>2</sub> nanowires at high (~950°C) and lower temperature (~700°C) with very high reproducibility, and a very large-scale SnO<sub>2</sub>NWs on Si and Al<sub>2</sub>O<sub>3</sub> substrates was obtained by that (see Fig. 10).

The screen-printing method for gas sensor device fabrication proposed in this work is very much simple, and a large number of devices were obtained as shown in Fig. 11. So this method is more efficient compared to that adopted by previous works. Fig. 11c represents current–voltage (I–V) characteristics of the gas sensor in air at different temperatures. The (I–V) curve of the as-fabricated gas sensor shows a good ohmic behavior. This points out that not only metal–semiconductor junction between the Au contact layer and SnO<sub>2</sub> NWs but also the semiconductor–semiconductor junction between the SnO<sub>2</sub> NWs are ohmic. The ohmic behavior is very important to the sensing properties, because the sensitivity of the gas sensor device is affected by contact resistance. Although there is large-number of gas sensor devices have been fabricated, only randomly selective devices were tested. Fig. 12a shows the responses of the SnO<sub>2</sub> NWs sensor under exposure to 10, 50 and 100 ppm of ethanol gas at 400°C. It can be seen that the resistance of the sensors in dry air is relatively large variation. This can be attributed to slightly difference in the NWs density and could be a disadvantage of the sensor fabrication method. However, the responses of the sensors are not much different as shown in Fig. 12b.

The latter issue is much more important for practical application than the former one. As also shown in Fig. 12b, the responses of all the measured sensors are increased linearly with increasing of concentration of ethanol gas with a small fluctuation. As-fabricated sensors were also tested with different gases such as CH<sub>3</sub>COCH<sub>3</sub>, C<sub>3</sub>H<sub>8</sub>, CO and H<sub>2</sub>. It can be seen that their response characteristics are very similar for the selected sensors. This is to suggest further that the sensor fabrication method in the present work is quite reproducible. Additionally, the responses to the measured gases of the sensors in the present work were used to extensively compare with the previous works. The responses ( $R_a/R_g$ ) to C<sub>2</sub>H<sub>5</sub>OH (100 ppm), CH<sub>3</sub>COCH<sub>3</sub> (100ppm), CO (100ppm), H<sub>2</sub> (100ppm) are round 11.8, 10.8, 2.9, and 3.4, respectively, which are comparable with most of the previous works [24]. The dynamic response transients were obtained for the SnO<sub>2</sub> NWs sensors. The 90% response time for gas exposure ( $t_{90\%(air-to-gas)}$ ) and that for recovery ( $t_{90\%(gas-to-air)}$ ) were calculated from the resistance–time data shown in Figure 12a. The  $t_{90\%(air-to-gas)}$  values in the sensing of 10, 50, and 100 ppm C<sub>2</sub>H<sub>5</sub>OH ranged from 4 to 6 s, while the  $t_{90\%(gas-to-air)}$  value ranged from 20 to 40s. More detail in this work can be found elsewhere [27].

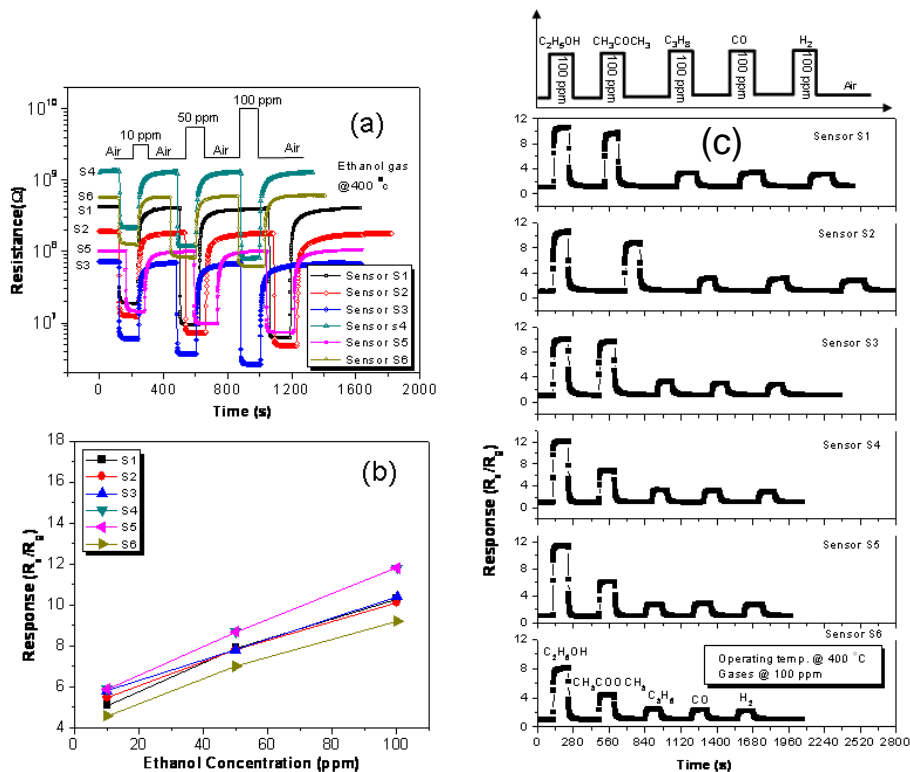


**Figure 12.** Response characteristic of randomly tested sensors to various ethanol concentrations at temperature of 400°C(a); response as a function of ethanol concentration (b); Transient response of randomly selected sensors to 100 ppm various gases (C<sub>2</sub>H<sub>5</sub>OH, CH<sub>3</sub>COOCH<sub>3</sub>, C<sub>3</sub>H<sub>8</sub>, CO, H<sub>2</sub>) (c) [27].

### 3.3. On-chip growth nanowires gas sensors.

The on-chip fabrication technique was applied for preparation of the SnO<sub>2</sub> NWs sensors designed for the detection of hydrogen concentrations ranging from 10 to 100 ppm and was found to be excellent in terms of performance [34]. This fabrication method overcame some problems faced when using the post-synthesis technique mentioned above. In addition, it was also found that it could scale-up the sensing elements and reduce the expenses of products. The on-chip fabrication method, however, has a limitation is that the

synthesis of most metal oxides nanowires is carried out at a high temperature that can degrade the metal electrodes (Pt) during sensor fabrication. In this study, we used the thermal evaporation as above to fabricate the on-chip SnO<sub>2</sub>-NWs gas sensors. The effect of growth time on structure and gas sensing properties of nanowires are investigated. In addition, the sensing mechanisms of SnO<sub>2</sub> nanowires gas sensors are also elucidated by comparing the sensing properties of on-chip fabrication sensor to those obtained using a screen-printing technique. The more detail about this work can found elsewhere [26].

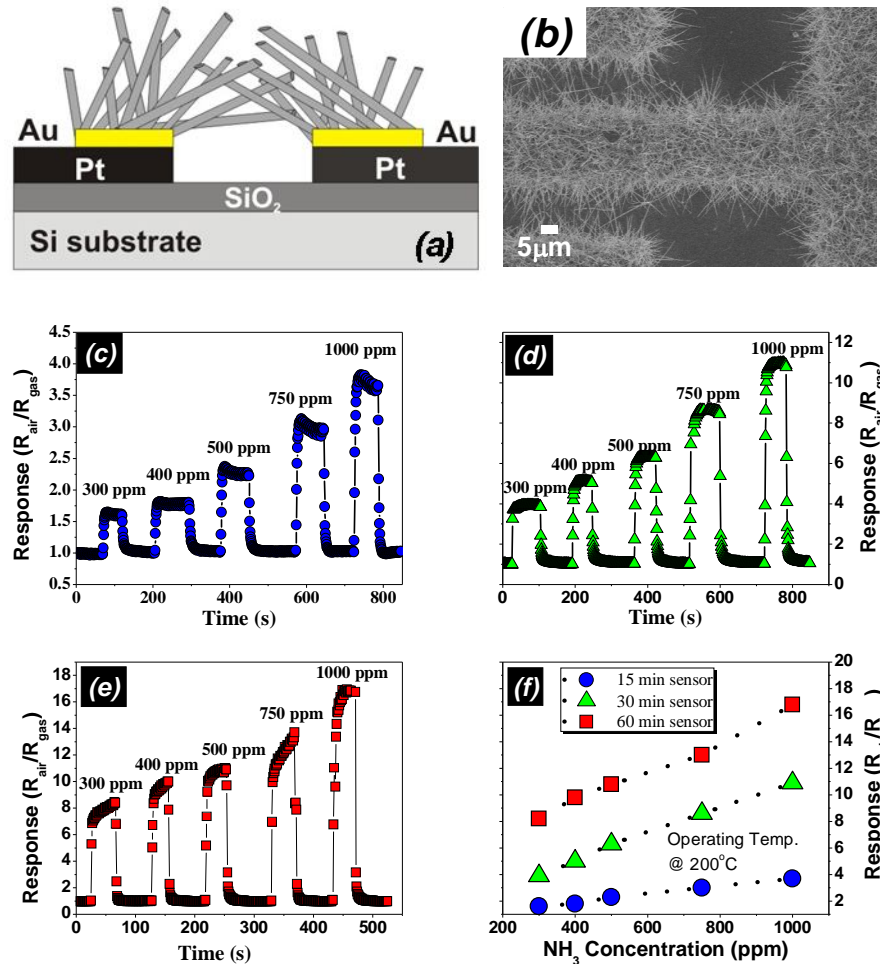


**Figure 13.** Schematic diagram of on-chip fabrication SnO<sub>2</sub> NWs sensors (a) typical SEM images of on-chip fabrication SnO<sub>2</sub> NWs grown for 15min (b); the change in response ( $R_{air}/R_{gas}$ ) upon exposure to different concentration of NH<sub>3</sub> measured at 200°C for nanowires grown at (a) 15min, (b) 30min, (c) 60min, a their response as a function of NH<sub>3</sub> concentration (d) [26].

The schematic diagram of the on-chip fabrication of SnO<sub>2</sub> NWs gas sensors is illustrated in Fig. 13a. Typical SEM image of as-obtained on-chip growth SnO<sub>2</sub> NWs sensor is shown in Fig. 13b. It can be seen that that the SnO<sub>2</sub> nanowires only grow in the substrate area where the Au catalyst is deposited. The silicon substrate can be seen clearly because there are no nanowires grown in the interspaces between

fingers of the Au/Pt electrode. These nanowires act as conducting lines for current flows during sensing measurements. The number of wire-wires contacts is increased with incase of growth time. The NH<sub>3</sub> sensing characteristics of sensors with growth time of 15, 30 and 60 min measured at the optimal working temperature of 200°C are shown in Fig. 13(c-e). The sensors showed very fast response and

recovery with a decrease in resistance upon exposure to  $\text{NH}_3$ . The sensor response increased with increasing growth time and so did response time. Fig. 13(d) summarizes the response of sensors grown at different time lengths as a function of  $\text{NH}_3$  concentration. All sensors showed a linear dependence of response to  $\text{NH}_3$  concentration ranging from 300 to 1000 ppm. The 60 min grown sensor had the highest response value of 8.2 to 300

ppm  $\text{NH}_3$ , followed by the 30 and 15 min grown sensors of 3.9 and 1.6, respectively.

### 3.4. Single nanowires gas sensor for ultrafast response and recovery

Recently, intensive efforts have been made to develop single NWs devices for gas sensing applications, because they can be used not only as resistive sensors, but also as field-effect sensors (see Fig.14a).

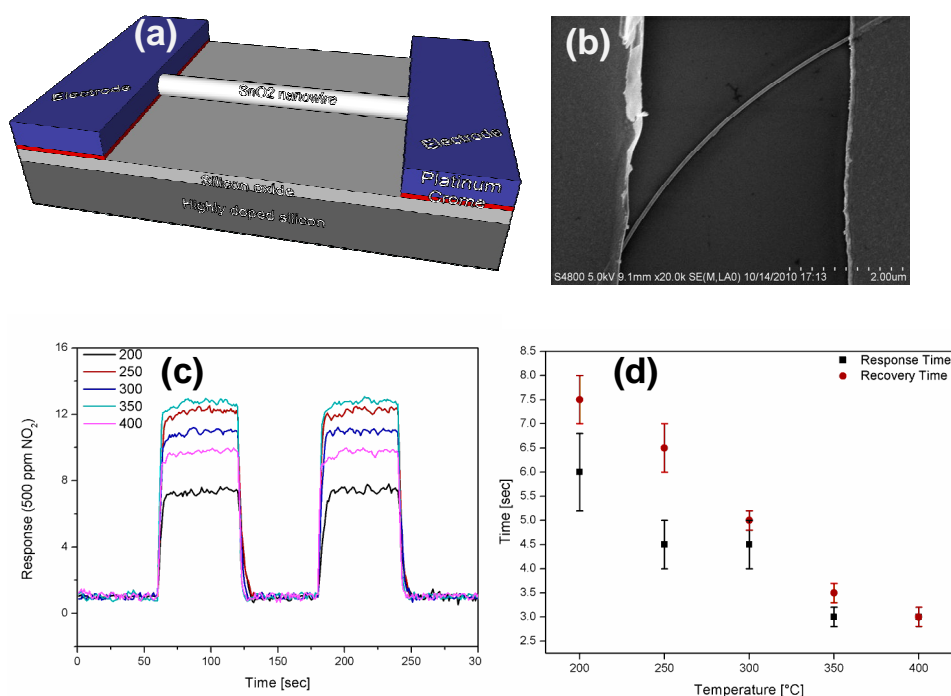


**Figure 14.** The configuration of single NWs gas sensor (a); As-fabricated SnO<sub>2</sub> NWs devices (b); the response to NO<sub>2</sub> at different temperatures (c); and the estimation of response-recovery time [32].

These sensors have pronounced good response and ultrafast response-recovery. Additionally, the self-heating effect can be applied for these kinds of sensors to operate at ultralow power consuming [35]. In previous works, complicated and expensive methods

such as ion beam lithography and focused ion beam have been used to fabricate the single nanowire devices. Our research is to develop a simple method to realize the single nanowires gas sensors. In brief, the SnO<sub>2</sub> NWs prepared on Si substrate by thermal evaporation was

used to disperse in isopropanol by ultrasonic for few seconds. The solution was dropped on SiO<sub>2</sub>/Si (i.e. 200 nm insulated SiO<sub>2</sub> film over Si substrate), and then Pt contact pads of 100 nm thickness were fabricated by UV lithography and rf sputtering. If the concentration of nanowires was optimized, we always could find a single nanowire between two electrodes with relatively high yield. A SEM image of the completed single SnO<sub>2</sub> NWs devices is typically shown in Figure 14b, in which a single SnO<sub>2</sub> NWs bridges two electrodes. The distance between the electrodes and diameter of SnO<sub>2</sub> NWs are about 5 μm and 10 nm, respectively. The gas-response of single NW sensor as shown in Figure 14a was measured with 500 ppm NO<sub>2</sub> gas at operating temperatures of 200-400°C with step of 50°C and its response showed in Fig. 14c. The optimum operating temperatures was about 350°C, where the response to 500 ppm NO<sub>2</sub> is about 12. The response and recovery times calculated from the transient response are shown in Figure 15d. It can be seen that they decrease with increasing operating temperature. At optimum operating temperature, the response and recovery times are 3 and 3.5 s, respectively. These values are much shorter than previous works [26-28].

### 3.5. SnO<sub>2</sub> nanowires functioned with catalytic materials

The selectivity and sensitivity of SnO<sub>2</sub> NWs sensors can be enhanced either by doping

with other oxide materials or by functionalizing with catalytically active materials [5]. We have developed a very simple route for functionalizing SnO<sub>2</sub> NWs. Herewith, we present our recent gas sensing properties of SnO<sub>2</sub> NWs for functionalizing SnO<sub>2</sub> NWs sensors with La<sub>2</sub>O<sub>3</sub> by solution deposition route. La<sub>2</sub>O<sub>3</sub> was selected as the catalytically active material because it has been reported to be a promising promoter for SnO<sub>2</sub>-based C<sub>2</sub>H<sub>5</sub>OH sensors. The morphology of SnO<sub>2</sub> NWs functionalized with La<sub>2</sub>O<sub>3</sub> using a 0.5M La(NO<sub>3</sub>)<sub>3</sub> solution was shown in Fig. 15. In the low magnification image (Fig. 15b), it was difficult to observe the La<sub>2</sub>O<sub>3</sub>-related phase. However, the second phases could be frequently found on the surface of SnO<sub>2</sub> NWs in the high-magnification SEM and TEM images (see arrows in Fig. 15c-15e), which were identified not as catalyst particles but as La<sub>2</sub>O<sub>3</sub> containing phase according to EDS analysis. Fig. 15f and 15h shows the responses to C<sub>2</sub>H<sub>5</sub>OH, CH<sub>3</sub>COCH<sub>3</sub>, C<sub>3</sub>H<sub>8</sub>, CO, and H<sub>2</sub> of the SnO<sub>2</sub> NWs sensor before and after La<sub>2</sub>O<sub>3</sub> doping using a 0.5M La(NO<sub>3</sub>)<sub>3</sub> aqueous solution. All the gas concentrations were fixed to 100 ppm for comparison. In the undoped SnO<sub>2</sub> NWs sensor, the responses ( $S=R_a/R_g$ ) to C<sub>2</sub>H<sub>5</sub>OH and CH<sub>3</sub>COCH<sub>3</sub> were 10.5 and 9.6, respectively. These responses are higher than those for C<sub>3</sub>H<sub>8</sub> ( $S = 3.3$ ), CO ( $S = 3.3$ ), and H<sub>2</sub> gases ( $S = 3.1$ ).

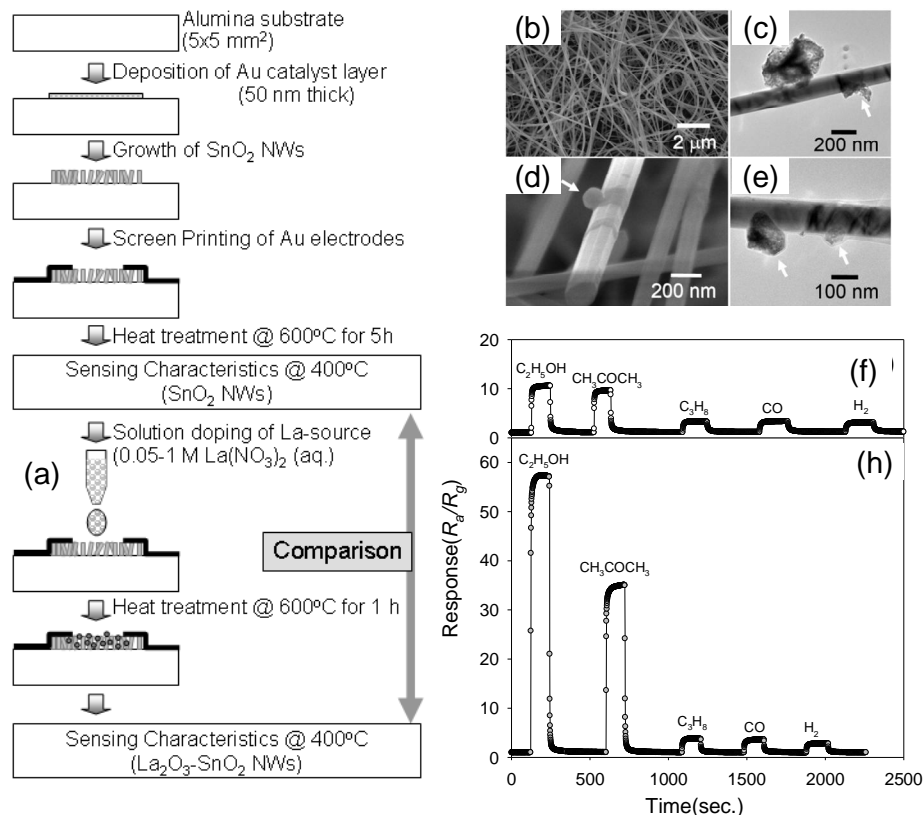


**Figure 15.** Schematic diagram of the sensor configuration and experimental procedures(a); SEM and TEM images of SnO<sub>2</sub> nanowires functionalized with La<sub>2</sub>O<sub>3</sub> using a 0.5M La(NO<sub>3</sub>)<sub>3</sub> solution after heat-treatment at 600°C for 5 h: (b) low resolution SEM image; (c) high resolution SEM image; and (d), (e) high resolution TEM images; gas responses to 100ppm of C<sub>2</sub>H<sub>5</sub>OH, CH<sub>3</sub>COCH<sub>3</sub>, C<sub>3</sub>H<sub>8</sub>, CO, and H<sub>2</sub> at 400°C of (e) undoped SnO<sub>2</sub> nanowires and (h) La<sub>2</sub>O<sub>3</sub>-doped SnO<sub>2</sub> nanowires using 0.5M La(NO<sub>3</sub>)<sub>3</sub> solution [21].

Therefore, the selective sensing of C<sub>2</sub>H<sub>5</sub>OH and CH<sub>3</sub>COCH<sub>3</sub> in the presence of C<sub>3</sub>H<sub>8</sub>, CO, and H<sub>2</sub> is possible. The responses to C<sub>2</sub>H<sub>5</sub>OH and CH<sub>3</sub>COCH<sub>3</sub> were increased to 57.3 and 34.9 by doping with La<sub>2</sub>O<sub>3</sub>, respectively, which are significantly higher than those of the pure SnO<sub>2</sub> NWs sensor. In contrast, the responses of the La<sub>2</sub>O<sub>3</sub>-doped SnO<sub>2</sub> NWs to C<sub>3</sub>H<sub>8</sub>, CO and H<sub>2</sub> were 3.8, 3.5, and 2.8, respectively, which are similar to the undoped SnO<sub>2</sub> NWs sensor. Further discussion

of this gas sensing property was reported in [28].

### 3.6. Gas-sensing mechanism of SMO nanowires sensors

Like most metal oxide semiconductor nanoparticles-based gas sensors, the sensing properties of 1D SMO nanostructures are attributed to oxygen molecules adsorbed on the surface of the SMO nanostructures which form O<sub>2</sub><sup>-2</sup> ions by capturing electrons from the

conductance band. So SMO nanostructures show a high resistance state in the air ambient. When SMO nanowires-based sensor is exposed to a reductive gas at moderate temperature, the gas reacts with the surface oxygen species of the nanowires, which decreases the surface concentration of  $O_2^{2-}$  ions and increases the electron concentration. This eventually increases the conductivity of the Q1D SMO nanostructures. However, in the case of SMO thin film, the charge state modification takes place only at the grain boundary or porous surface. In the case of Q1D SMO nanostructures, it is expected that the electronic transport properties of the entire Q1D SMO

nanostructures will change effectively due to the gas adsorption. The Debye length  $\lambda_D$  (a measure of the field penetration into the bulk) for most semiconducting oxide nanowires is comparable to their radius over a wide temperature and doping range, which causes their electronic properties to be strongly influenced by processes at their surface. As a result, one can envision situations in which a nanowire's conductivity could vary from a fully nonconductive state to a highly conductive state entirely on the basis of the chemistry transpiring at its surface. This could result in better sensitivity and selectivity.

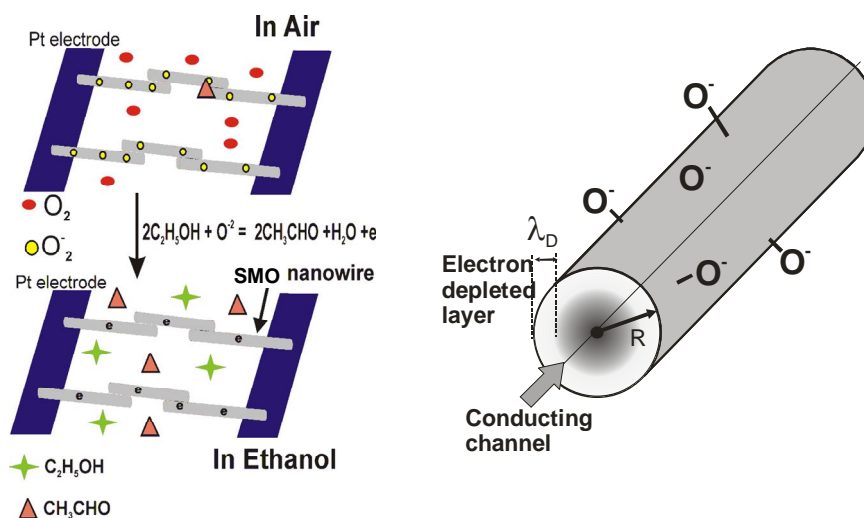


Figure 16. Summaries of gas sensing mechanism of SMO nanowires.

#### 4. CONCLUSION

A survey of preparation techniques, physical and chemical properties, and performances of SMO/CNTs hybrid materials and 1D SMO gas sensors have been presented. Alternative hybrid materials have been

developed for gas-sensing applications. We have focused our attention to reduction of operating temperature of SMO-based sensor by doping CNTs and development of room temperature gas sensors for  $NH_3$  detection. SMO co-doped with CNTs and catalytic

materials seems efficient route to enhance gas-sensing performance of SMO-based sensors.

We have also intensively paid attention to synthesis and fabrication of SMO nanowires-based sensors. It is very promising for better understanding of sensing principles and development of a new generation of sensors. The selectivity of course still remains a concern for metal oxide based gas sensor. This may be improved by fabricating sensor arrays using several doping nanowires, or by functionalization of their surfaces that has been demonstrated in this work.

Still a great need of controlling in the growth is required for an application of those class materials in commercial systems, together with a thorough understanding of the growth

mechanism that can lead to a control in nanowires size and size distributions, shape, crystal structure and atomic termination. A great attention has to be paid to problems like the electrical contacts and nano-manipulation that allow production and integration of gas sensor devices.

#### ACKNOWLEDGEMENT

This research is funded by Vietnam National Foundation for Science and Technology Development (NAFOSTED) under grant number 103.02-2011.40.

### TỔNG QUAN CÁC NGHIÊN CỨU CỦA CHÚNG TÔI VỀ VẬT LIỆU NANO CHO CẢM BIẾN KHÍ

Nguyễn Văn Hiếu<sup>(1)</sup>, Hoàng Sĩ Hồng<sup>(2)</sup>, Đỗ Đăng Trung<sup>(1)</sup>, Bùi Thị Thanh Bình<sup>(1)</sup>, Nguyễn Đức Chính<sup>(1)</sup>, Nguyễn Văn Duy<sup>(1)</sup>, Nguyễn Đức Hòa<sup>(1)</sup>

(1) Viện Đào Tạo Quốc Tế Về Khoa Học Vật Liệu (ITIMS), Trường Đại Học Bách Khoa Hà Nội

(2) Viện Điện, Trường Đại Học Bách Khoa Hà Nội

**TÓM TẮT:** Trong thời gian gần đây các loại vật liệu có cấu trúc nano như nano oxit kim loại bán dẫn (SMO), ống nano carbon (CNTs) và vật liệu lai SMO/CNTs được quan tâm nhiều trong lĩnh vực cảm biến khí. Đây là những hệ vật liệu tiềm năng trong ứng dụng làm cảm biến khí nhằm cải thiện ba đặc trưng quan trọng của cảm biến khí đó là “độ nhạy”, “độ chọn lọc” và “độ ổn định” (3S). Công trình này sẽ trình bày các kết quả nghiên cứu gần đây của chúng tôi về việc tổng hợp, khảo sát tính chất về cấu trúc và tính chất nhạy khí của một số hệ vật liệu nano. Chúng tôi tập trung vào hai hệ vật liệu là (i) vật liệu lai giữa CNTs/SMO và (ii) loại cấu trúc nano một chiều oxit kim loại bán dẫn. Cỡ chế nhạy

khí và khả năng phát triển các hệ vật liệu nano mới nhằm ứng dụng cho cảm biến khí cũng sẽ được bàn luận.

**Từ khóa:** Ống nano carbon, dây nano, vật liệu lai, cảm biến khí.

#### REFERENCES

- [1]. E. Comini, Metal oxide nano-crystals for gas sensing, *Analytica Chimica Acta* 568, 28–40 (2006).
- [2]. X.-J. Huang, Y.-K. Choi, Chemical sensors based on nanostructured materials, *Sens. Actuators B* 122 659–671 (2007).
- [3]. A. Modi, N. Koratkar, E. Lass, B. Wei, Miniaturized gas ionization sensors using carbon nanotubes, *Nature* 424, 171-173 (2003).
- [4]. T. Someya, J. Small, P. Kim, C. Nuckolls, and J. T. Yardley, Alcohol vapor sensors based on single-walled carbon nanotube field effect transistors, *Nano Lett.* 3, 877-881(2003).
- [5]. A. Kolmakov and M. Moskovits, Chemical sensing and catalysis by one-dimensional metal-oxide nanostructures, *Annu. Rev. Mater. Res.* 34, 51–80(2004).
- [6]. U. Lange, N.V. Roznyatovskaya, V.M. Mirsky, Conducting polymers in chemical sensors and arrays, *Analytica Chimica Acta*, 614, 1-26 (2008).
- [7]. J. Gong, J. Sun, Q. Chen, Micromachined Sol-Gel carbon nanotube/SnO<sub>2</sub> nanocomposite hydrogen sensor, *Sens. Actuators B* 30, 829-835(2008).
- [8]. W.-Q. Han and A. Zettl, Coating single-walled carbon nanotubes with tin oxide, *Nano Lett.* 3, 681-683 (2003).
- [9]. B.-Y. Wei, M.-C. Hsu, P.-G. Su, H.-M. Lin, R.-J. Wu, H.-J. Lai, A novel SnO<sub>2</sub> gas sensor doped with carbon nanotubes operating at room temperature, *Sens. Actuators B* 101, 81–89 (2004).
- [10]. A. Wisitsoraat, A. Tuantranont, C. Thanachayanont, V. Patthanasettakul, P. Singjai, Electron beam evaporated carbon nanotubes dispersed SnO<sub>2</sub> thin films gas sensor, *J. Electroceram*, 17, 45-47 (2006).
- [11]. C. Bittencourt, A. Felten, E.H. Espinosa, R. Ionescu, E. Llobet, X. Correig, J.-J. Pireaux, WO<sub>3</sub> films modified with functionalized multi-wall carbon nanotubes: Morphology, compositional and gas response, *Sens. Actuators B* 115, 33-41(2006).
- [12]. E.H. Espinosa, R. Ionescu, B. Chambon, G. Bedis, E. Sotter, C. Bittencourt, A. Felten, J.-J. Pireaux, X. Correig, E. Llobet, Hybrid metal oxide and multiwall carbon nanotube films for low temperature gas sensing, *Sens. Actuators B* 127, 137-142 (2007).
- [13]. J.G. Lu, P. Chang, Z. Fan, Quasi-one-dimensional metal oxide materials-synthesis, properties and applications, *Mater. Sci. Eng. R* 52, 49–91 (2006).

- [14]. A. Kolmakov, M. Moskovits, Chemical sensing and catalysis by one-dimensional metal-oxide nanostructures, *Ann. Rev. Mater. Res.* 34, 150–180 (2004).
- [15]. X.-J. Huang, Y.-K. Choi, Chemical sensors based on nanostructured materials, *Sens. Actuators B*, 122, 659–671 (2006).
- [16]. N.V. Hieu, N.V. Duy, N.D. Chien, Inclusion of SWCNTs in Nb/Pt co-doped TiO<sub>2</sub> thin film sensor for ethanol vapor detection, *Physica E*, 40, 2950-2958 (2008).
- [17]. N.V. Hieu, N.A.P. Duc, T. Trung, M.A. Tuan, N.D. Chien, Gas-sensing properties of tin oxide doped with metal oxides and carbon nanotubes: A competitive sensor for ethanol and liquid petroleum gas, *Sens. Actuators B*, 144, 450–456 (2010).
- [18]. N.V. Duy, N.V. Hieu, P.T. Huy, N.D. Chien, M. Thamilselvana, Junsin Yia, Mixed SnO<sub>2</sub>/TiO<sub>2</sub> included with carbon nanotubes for gas sensing application, *Physical E: Low-dimensional Systems and Nanostructures*, 41, 258-263 (2008).
- [19]. N.V. Hieu, L.T.B. Thuy, N.D. Chien, Highly sensitive thin film NH<sub>3</sub> gas sensor operating at room temperature based on SnO<sub>2</sub>/MWCNTs composite, *Sens. Actuator B*, 129, 888-895 (2008).
- [20]. N.V. Hieu, N.Q. Dung, T. Trung, N.D. Chien, Thin film polypyrrole/SWCNTs nanocomposites-based NH<sub>3</sub> sensor operated at room temperature, *Sens. Actuators B*, 140, 500-507 (2009).
- [21]. N.V. Hieu, H.-R. Kim and J.-H. Lee, The enhanced gas sensing characteristics of La<sub>2</sub>O<sub>3</sub>-doped SnO<sub>2</sub> by the addition of multi wall carbon nanotubes, *Sensor Lett.* 9, 283-287 (2011).
- [22]. P.D. Tam, M.A. Tuan, L.A. Tuan, N.V. Hieu, Facile preparation of a DNA sensor for rapid herpes virus detection, *Mater. Sci. Eng. C*, 30, 1145-1150 (2010).
- [23]. P.D. Tam, N.V. Hieu, Conducting polymer film-based immunosensors using carbon nanotube/antibodies doped polypyrrole, *Applied Surface Science*, 257, 9817-9824 (2011).
- [24]. N.V. Hieu, N. Duc Chien, Low Temperature Growth of Q1D-ZnO Nanostructures for Gas Sensing Application, *Physical B*, 403, 50-56(2008).
- [25]. N.V. Hieu, D.T.T. Le, L.T.N. Loan, N.D. Khoang, N.V. Quy, N.D. Hoa, P.D. Tam, A.-T. Le, T. Trung, A comparative study on the NH<sub>3</sub> gas-sensing properties of ZnO, SnO<sub>2</sub>, and WO<sub>3</sub> nanowires, *Int. J. Nanotechnology*, 8, 174-187 (2011).
- [26]. L.V. Thong, N.D. Hoa, D.T.T. Le, D.T. Viet, P.D. Tam, A.T.-Le, and N.V. Hieu, On-chip fabrication of SnO<sub>2</sub>-nanowire gas sensor: The effect of growth time on sensor

- performance, *Sens. Actuators B*, 146, 361-367 (2010).
- [27]. N.V. Hieu, Highly reproducible synthesis of very large-scale tin oxide nanowires used for screen-printed gas sensor, *Sens. Actuators B*, 144, 425-431 (2010).
- [28]. N.V. Hieu, H.-R. Kim, B.-K. Juc and J.-H. Lee, Enhanced performance of SnO<sub>2</sub> nanowires ethanol sensor by functionalizing with La<sub>2</sub>O<sub>3</sub>, *Sens. Actuator B*, 133, 228-234 (2008).
- [29]. N.D. Hoa, N.V. Quy, M.A. Tuan, N.V. Hieu, Facile synthesis of p-type semiconducting cupric oxide nanowires and their gas sensing properties, *Physica E*, 42, 146-149 (2009).
- [30]. N.V. Hieu, V.V. Quang, N.D. Hoa, D. Kim, Preparing large-scale WO<sub>3</sub> nanowire-like structure for high sensitivity NH<sub>3</sub> gas sensor through a simple route, *Current Appl. Phys.* 11, 657-661 (2011).
- [31]. L.V. Thong, L.T.N. Loan, N.V. Hieu, Comparative study of gas sensor performance of SnO<sub>2</sub> nanowires and their hierarchical nanostructures, *Sens. Actuators B* 112, 112-119 (2010).
- [32]. M. Tonzzer and N.V. Hieu, Size-dependent response of single-nanowire gas sensors, *Sens. Actuators B*, 163, 146-152 (2012).
- [33]. D.R. Patil, L.A. Patil, and P.P. Patil, Cr<sub>2</sub>O<sub>3</sub>-activated ZnO thick film resistors for ammonia gas sensing operable at room temperature, *Sens. Actuators B*, 126, 368-374 (2007).
- [34]. B. Wang, L.F. Zhu, Y.H. Yang, N.S. Xu, G.W. Yang, Fabrication of a SnO<sub>2</sub> nanowires gas sensor and sensor performance for hydrogen, *J. Phys. Chem. C* 112, 6643-6647 (2008).
- [35]. D. Prades, R.J.-Diaz, F.H.-Ramirez, S. Barth, A. Cirera, J. D. Prades, J.-Diaz, F. H.-Ramirez, S. Barth, A. Cirera, Ultralow power consumption gas sensors based on self-heated individual nanowires, *Appl. Phys. Lett.* 93, 123110-3 (2008).